Silvan Kuttimalai

Resolution Measurements

With the Eudet Pixel Telescope

D
E
S
Y

Summer School Program 2011

Abstract

In this report, the resolution studies that were conducted during the 2011 DESY summer school program are presented. The pointing resolution as well as the sensor resolution of the EUDET pixel telescope is determined for six threshold settings. These measurements are based on data taken during a two week period at the CERN SPS test beam line using a pion beam with particle energies of 120 GeV. Using a copy of the EUDET telescope currently located at the DESY II test beam, data was also taken with a low energy electron beam. At the time of the end of the program, this data was not fully reconstructed and therefore, the presented results will be restricted to data taken at CERN, Geneva.

Contents

1 Introduction

In this report, resolution studies with the EUDET pixel telescope are presented. The corresponding measurements were conducted during the 2011 summer student program of DESY, Hamburg. This program gives undergraduate students the opportunity to participate in research activities of DESY scientists and offers a variety of lectures given by leading researchers in the filed of high energy physics, particle accelerator and detector development, photon science, as well as astrophysics.

My work at DESY was supervised by Ingrid-Maria Gregor and the measurements were conducted in close collaboration with Cora Fischer and Ilya Khvastunov who were concerned with the assessment of the mechanical stability of the telescope setup, measurements of the telescope sensor's efficiency, as well as the determination of the fake hit rate.

2 EUDET - Detector Research and Development towards the International Linear Collider

The International Linear Collider (ILC), a proposed linear electron-positron collider, is in its current technical design phase intended to provide measurements of unprecedented accuracy and precision. The design concept of the ILC therefore demands for sophisticated detector technologies to be developed. Due to the fundamental differences between hadron and lepton colliders, the requirements for future ILC detectors are at odds with technologies developed for the Large Hadron Collider especially in terms of precision, resolution power, and material budget.

EUDET is a project funded by the European Union and coordinated by DESY that was launched in 2005 and successfully completed in 2010. It aimed at the coordination of a joint European effort towards research and development for future particle detectors that meet the requirements of a future linear lepton collider. Part of the EUDET project was the establishment of three dedicated joint research activities (JRA) working on the improvement and maintenance of the necessary infrastructure for detector research and development. Aiming specifically at test beam infrastructures for precision tracking devices, a pixel telescope was developed within JRA 1. This device was subject to the resolution studies that are presented in this report. It will be described in more detail in section 3.

3 The EUDET Pixel Telescope

3.1 Overview

In the process of tracking detector development, newly constructed devices need to be characterized in terms of resolution power and efficiency. Dedicated test beam facilities provide energetic charged particles that are used for this purpose. In order to extract the parameters of interest from measurements with the device under test (DUT), one needs to determine the tracks of the used test beam particles very precisely. Beam telescopes are usually used to achieve this. Placing both the telescope and the DUT in the test beam, one

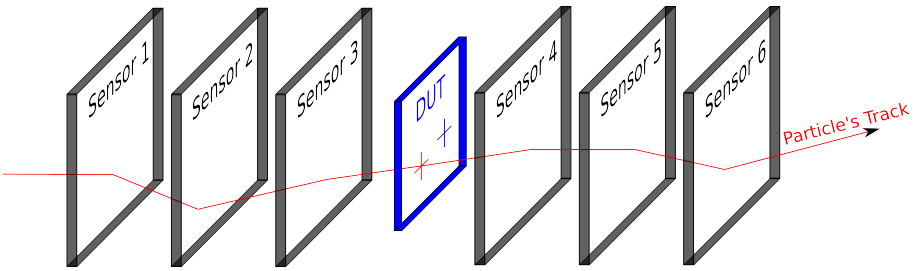

Figure 1: Schematic diagram of the pixel telescope. The beam particles travel along the positive z direction. This convention will be used throughout this report.

can precisely measure tracks of incoming particles and study the response of the DUT for example in terms of the resolution capacity.

The design requirements for a beam telescope to be build within the EUDET project [1] comprised flexibility and portability to make it usable at the low momentum electron test beam line at DESY as well as at the high momentum hadron test beams at CERN. Furthermore, the telescope needed to be compatible with a wide variety of DUTs, providing an easy-to-use interface and data acquisition system that requires only a minimum amount of adjustments to incorporate different DUTs. The design requirements concerning the resolution power were such that the impact position on the DUT needs be predicted by the telescope with a precision of less than 3 µm, even at the low energy electron beam where multiple scattering processes have a significant impact on the resolution power. Based on resolution studies [2] it was decided to choose a telescope geometry layout depicted in figure 1 with two telescope arms, each one housing three pixel sensors that are aligned perpendicular to a common beam axis. With this setup and the DUT being placed between the two telescope arms, the impact position at the DUT plane can be inferred from a track fit using the combined measurements in all six telescope planes. Figure 3 shows all the infrastructure elements required for the operation of the telescope and data acquisition. Each of these components will be discussed in detail in sections 3.2 to 3.7.

3.2 Mechanical Setup

The support frame that holds all telescope components in place is built our of rigid aluminum construction profiles. It provides support for the two telescope arms, the DUT, cables, cooling system components and parts of the readout electronics. The two arms of the telescope are equipped with a rail system on which the sensor jigs that house the pixel sensors are guided. This rail system allows for precise adjustments of the telescope's geometric setup and the distance between two adjacent sensors on one arm can be varied within a range of 20 to 150 mm. Between the telescope arms there is sufficient space to allow for the installation of DUTs up to a size of 50 cm. With an optional precision x-y-ϕ-actuator table one can move a DUT through the active area between the telescope arms in the x-y-plane perpendicular to the nominal beam

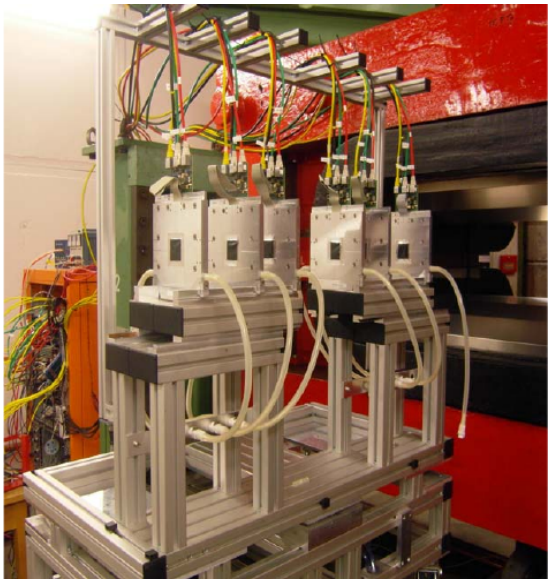

Figure 2: Photograph of the pixel telescope installed at the DESY-II test beam with no DUT.

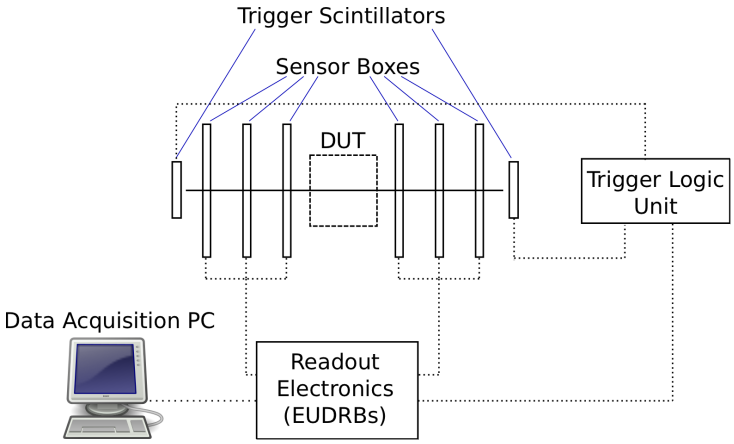

Figure 3: Schematic diagram of all components necessary for operating the beam telescope.

direction. Linear displacements as well as rotations in this plane are possible.

3.3 Pixel Sensors

The telescope is equipped with Mimosa26 CMOS pixel sensors. CMOS pixel sensors detect minimum ionizing particles by collecting the charge liberated when such a particle traverses the sensor. The charge is released in an almost undepleted so-called epitaxial layer on the wafer substrate. The charge is the collected by evenly distributed n-type doped wells that are implemented in such a way that they are in direct contact with the p-type epitaxial layer.

The overall thickness of the sensor is 50 µm and due to the fine granularity with a pixel pitch of 18.4 µm, single point resolutions better that 4 µm can be achieved. Depending on the threshold settings of the sensors, the sensor resolution can vary though. The threshold setting is parametrized by a dimensionless quantity S/N that is closely related to the amount of charge that needs to be collected by a pixel before it fires [3]. The cluster sizes and the spatial distributions of pixels making up the individual clusters (see section 3.7 for some details) will of course be affected by the threshold settings. Therefore, the accuracy of the hit positions that are calculated from the cluster topology will depend on the threshold settings, thereby also affecting the resolution power.

3.4 Trigger System

The entire telescope system is triggered by a trigger logic unit (TLU) developed within the JRA 1 program [4]. This unit receives signals from two scintillators, one of them being installed in front of the sensor closest to the beam source and on being placed behind the telescope. From the scintillator signals the TLU generates triggers that are received by both the telescope and the DUT. Furthermore, there are several so-called handshake modes for DUT integration available in which the DUT can respond to a trigger signal by sending a busy signal back to the TLU that is dropped when the DUT is ready for another trigger pulse. This ensures that the telescope system is only triggered when all devices are actually ready for readout.

3.5 Readout Electronics

Custom made readout electronic has been developed to read out the digital Mimosa26 sensors. Initially designed for the readout of the analogue sensors of a provisional telescope that was established prior to the final version that we studied, the “EUDRBs” (EUDET data reduction boards [5]) have been adapted to handle the digital signals of the Mimosa26 sensors.

3.6 Data Acquisition

The EUDAQ software is a software framework specifically designed to provide a lightweight and portable user interface for convenient data acquisition [6]. The architecture is structured in several distinct so-called “producers”:

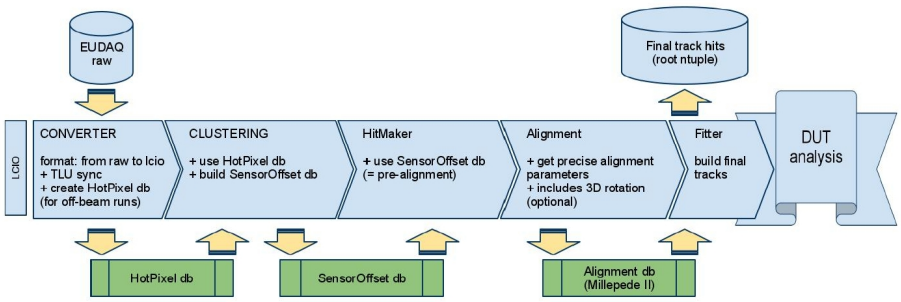

Figure 4: Workflow diagram for the full analysis procedure.

Run Control The run control is the central graphical interface. The user can control the process of data acquisition using this producer and also monitor the status of all other software components.

TLU Producer The trigger logic unit can be controlled via the TLU producer. This component also receives all the TLU output data necessary for a complete event data stream building such as time stamps and run numbers.

Data Collector The data collector receives data from multiple software components such as the TLU producer but also from the data reduction boards in order to merge all necessary data streams for the final raw data storage on disk.

Online Monitor Since real-time monitoring of the recorded data is very convenient, the online monitor was implemented. This producer reads the data recorded on disk and provides the user with a set of histograms and plots that indicate the potential misalignment of sensors and various other observables.

Log Collector The log collector organizes log messages from all software components in such way that its easy for the user to keep track of the overall status of the data acquisition software.

3.7 Offline Event Reconstruction

For the offline event and track reconstruction the dedicated software package EUTelescope is available [7, 8]. This package is based on the highly modular Marlin framework that was designed for a future linear collider [9]. EUTelescope comprises a bundle of so-called Marlin "Processors" each one of which performs a certain dedicated task in the analysis chain, thereby exploiting the modularity of Marlin. Figure 4 shows a diagrammatic representation of all the necessary steps towards completely reconstructed events. In what follows, these steps will be briefly discussed except for the track fitting procedure. The track fit is of major importance for the performed analysis, therefore it will be covered separately in section 3.8.

File Conversion Since Marlin relies on the "LCIO" data format of the LCIO persistency framework and event data model, the raw data that was written by the EUDAQ software needs to be converted.

Clustering Depending on the threshold settings of the sensors, the number of pixels firing when a particle traverses a sensor is in general larger than one. Therefore, nearby firing pixels that are likely to belong to one common hit need to be grouped to clusters. In our analysis, we used a sparse clustering algorithm with non-fixed cluster size and shape implemented in EUTelescope. A scan of the entire sensor in search for "seed pixels" with a signal strength above a certain threshold that is defined by the user is performed first. Then, pixels within a predefined vicinity are added to a cluster if their signal strength exceeds a user defined threshold.

Hit Maker Once the hit clusters have been identified, particle impact positions have to be inferred from those clusters. The "charge center of gravity" is calculated by computing the signal weighted average position of the cluster. In order to account for nonlinear charge collection effects within one pixel, a so-called η-correction is applied. Without this correction the obtained positions are not evenly distributed within a pixel although the actual impact positions of course are evenly distributed.

Alignment Since the telescope geometry can mechanically only be adjusted up to an accuracy significantly larger than the desired resolution, the deviations between the nominal sensor positions and the actual sensor positions need to be corrected for. The EUTelescope software uses "Millepede II" [10] for the determination of the misalignment of the sensors. A rough track fit procedure is performed and the alignment parameters are calculated from the resulting tracks. Among the alignment parameters are shifts and rotations of the sensors in the x-y-plane as well as angles of rotation around the x and y axes.

3.8 Analytic Track Fitting

The particle tracks that penetrate the telescope's sensors are subject to scattering processes in the sensors and therefore do not pass straight through the telescope. The track fit performed in the last step of the analysis chain takes into account both the measured hit positions and the expected scattering angle distribution. Most of the deflection of the particle's trajectories when traversing the sensor material is due to Coulomb scattering. For scattering angles as small as they can be expected to be for the sensor thickness of 50 µm, the distribution of the scattering angles is approximately Gaussian. This also holds approximately for the projections of the scattering angle onto the x-z- and the y-z-plane. The width of this distribution is given in terms of the sensor thickness d, the sensor material's radiation length X_0, the velocity βc, and the momentum p of the beam particles [11]:

$$\sigma_\theta = \frac{13.6\,\mathrm{MeV}}{\beta c p}\sqrt{\frac{d}{X_0}}\left[1 + 0.038\ln\left(\frac{d}{X_0}\right)\right] \tag{1}$$

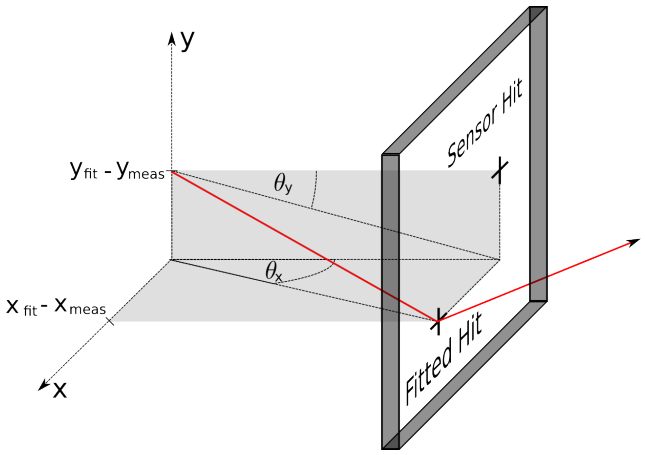

Figure 5: Definition of the projected scattering angles. The angles displayed correspond to the sensor index i while sensor and sensor hit positions correspond to the index $i+1$.

This relation is valid for singly charged particles. For particles with charge number Z, expression (1) must be multiplied by Z.

The track fit from which the hit positions x^i_{fit} and y^i_{fit} in the individual planes ($i \in \{1, 2, ..., N\}$ for N telescope sensor planes) are obtained is performed via a χ^2 minimization. The χ^2 function that correctly takes into account both the measurements x^i_{meas} and y^i_{meas} as well as the expected scattering angle distributions is given by a sum of two contributions corresponding to the x-coordinates and the y-coordinates:

$$\chi^2 = \chi^2_x + \chi^2_y \tag{2}$$

χ^2_x is given in terms of the telescope's sensor resolution σ_s and the expected scattering angle spread that can be computed from (1):

$$\chi^2_x = \sum_{\substack{i=1 \\ i \neq i_{\text{DUT}}}}^{N} \left(\frac{x^i_{\text{meas}} - x^i_{\text{fit}}}{\sigma_{\text{s}}} \right)^2 + \sum_{i=2}^{N-1} \left(\frac{\theta^i_x - \theta^{i-1}_x}{\sigma^i_\theta} \right)^2 \tag{3}$$

The y-contribution to χ^2 can be computed analogously and therefore the following considerations will be restricted to the x-direction. The first sum in (3) accounts for the measurements of the telescope sensors while the second sum factors in the expected scattering angle distribution. The scattering angle projections θ^i_x and θ^i_y are defined in figure 5. From equation (1) one can calculate the magnitude of typical scattering angles that are to be expected. Plugging in the parameter values of the Mimosa26 sensors and the radiation length of silicon $X_0 \approx 13.6\,\text{mm}$ one obtains $\theta_0 \approx 2 \times 10^{-6}\,\text{rad}$. For such small angles, the projected scattering angles can be approximated very well by

$$\theta^i_x \approx \frac{x^{i+1}_{\text{fit}} - x^i_{\text{fit}}}{z^{i+1} - z^i} \tag{4}$$

where z^i is the position of sensor i along the nominal beam axis. Applying the approximation (4) to the (3), the resulting χ^2 becomes quadratic in all degrees of freedom, that is, the hit positions x^i_{fit} and y^i_{fit}. Because of dependencies are of solely quadratic nature, the minimum of χ^2 can be found analytically. Finding the minimum of χ^2 (or demanding the derivatives of χ^2 with respect to all x^i_{fit} to vanish) is equivalent to finding a solution to the matrix equation

$$\sum_{i=1}^{N} \mathcal{M}_{ij} x^i_{\text{fit}} = \varepsilon^j x^j_{\text{meas}} \tag{5}$$

where

$$\mathcal{M}_{ij} = \frac{1}{2} \frac{\partial^2 \chi^2}{\partial x^i_{\text{fit}} \partial x^j_{\text{fit}}} \tag{6}$$

$$\varepsilon^j = \begin{cases} 1/\sigma_{\text{s}}^2 & \text{if } j \neq j_{\text{DUT}} \\ 0 & \text{if } j = j_{\text{DUT}} \end{cases} \tag{7}$$

Therefore, the most probable track can be found by inverting the matrix $\mathcal{M}$ and solving equation (5) for all x^i_{fit}. Since the only parameters that enter χ^2 are telescope parameters such as the z positions of the sensors and the DUT, their thicknesses and the sensor resolution σ_s, the matrix needs to be inverted only once. Furthermore, the expected accuracy of the track fit can also be computed from the telescope parameters that enter the χ^2 function since the covariance matrix is given by the inverse $\mathcal{M}^{-1}$. The expected error on the fitted impact position of a track in the i^{th} plane is given by

$$\sigma^i_{\text{fit}} = \sqrt{(\mathcal{M}^{-1})_{ii}} \tag{8}$$

Since this quantity gives the expected accuracy of the impact position prediction based on the telescope's measurement and because it depends only on telescope parameters, it is referred to as the telescope's pointing resolution σ_{tel}:

$$\sigma_{\text{tel}} := \sigma_{\text{fit}} \tag{9}$$

4 Measuring the Telescope's Pointing Resolution

The ultimate goal of the presented analysis is the determination of the telescope's pointing resolution and it's dependence on the threshold settings of the telescope sensors. In section 4.1, the measurement strategy will be discussed. Some details on the data acquisition at the CERN and DESY test beams will be given in 4.2

4.1 Extracting the Pointing Resolution from Residual Distributions

In order to measure the resolution power of the telescope, we performed a series of experiments in which the so-called residual distribution was measured. The

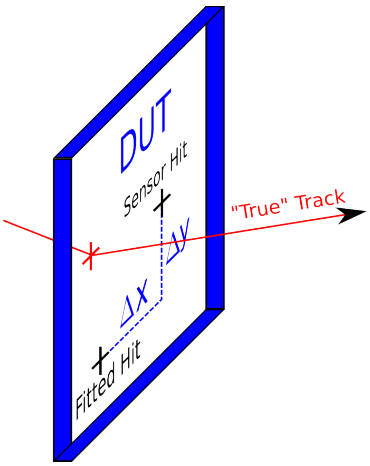

Figure 6: Definition of the residuals Δx and Δy. In General, the true hit position will differ from both the DUT sensor hit and the hit predicted by the telescope's track fit.

distribution of the x residuals is the distribution of deviations between the hit position at the DUT plane measured by the DUT itself x_{meas} and the fitted hit position predicted by the telescope x_{fit}. Figure 6 illustrates this quantity with an example showing the x residual Δx as well as the y residual Δy. In what follows, the considerations will again be limited to the x direction but the discussion is without any constraints also valid for the y direction. The distribution of the residuals Δx is for now assumed to be Gaussian which is eventually to be validated by the measurements presented in this report. The width of the Gaussian distribution σ_{tot} receives contribution from two sources. On the one hand there is the expected deviation between the true track hit and the prediction inferred from the track fit. An estimate an the most probable value of this deviation is given by (8) as discussed in section 3.8. On the other hand there is the expected deviation between the true track hit and the hit position measured by the DUT. This quantity is referred to as the resolution σ_{DUT} of the DUT. Both contributions combine quadratically to give the total residual width:

$$\sigma_{\text{tot}}^2 = \sigma_{\text{tel}}^2 + \sigma_{\text{DUT}}^2 \tag{10}$$

Equation (10) gives an analytic expression for the total residual width one would measure in experiment with the sensor resolutions σ_{s} and σ_{DUT} as the only unknown parameters. Since the telescope geometry and the sensor thicknesses are known, σ_{tel} does only depend on σ_{s} as discussed in section 3.8. The expression for the total residual width becomes even more simpler if one measures the distribution using one of the telescope sensors instead of integrating a DUT with a resolution different from σ_s. An experimental setup following that strategy is depicted in figure 7. Declaring the telescope sensors a DUT, one can obtain six residual distributions by repeating the measurement six times where each of the telescope sensors is treated as a DUT once. The actual data taking does not need to be repeated though.When declaring different sensors a DUT, the only adaption necessary is changing the DUT sensor index in the track fit procedure. With the residual distribution measured in one of the sensor planes, the expression for the analytic evaluation of the distribution width simplifies

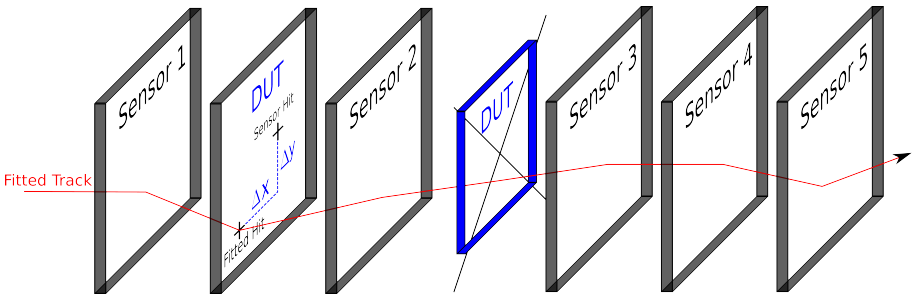

Figure 7: Instead of inserting an additional DUT, the residual distributions are measured in the telescope planes.

to

$$\sigma_{\text{tot}}^2 = \sigma_{\text{tel}}^2(\sigma_{\text{s}}) + \sigma_{\text{s}}^2 \tag{11}$$

In equation (11) the dependence on σ_{s} is written explicitly in order to stress that this is the only unknown parameter. Finally, having measured the six individual residual distributions, one can perform a fit with all six obtained residual widths corresponding to the six sensor in order to extract σ_{s}, which in turn also gives the telescope's pointing resolution σ_{tel}.

4.2 Data Acquisition

Initially it was planned measure the telescope's resolution in a wide range of particle energies and for six different threshold settings $S/N \in \{5, 6, 7, 8, 9, 10\}$. The data was taken not only at the DESY II test beam line [12], where currently a copy of the EUDET telescope by the name of "ANEMONE" is installed, but also with the original EUDET telescope located at one of the SPS test beam lines at CERN in Geneva [13]. The telescope at CERN was controlled remotely via the web using computers in the DESY test beam control room. While at the SPS test beam lines there are electron and hadron beams in a wide energy range up to several hundred GeV available, the DESY II test beam delivers electrons or positrons with energies between 1 GeV and 6 GeV. During our data acquisition period the CERN test beam delivered pions, while at DESY we took data using an electron beam. Both test beams are secondary beams. At the electron/positron synchrotron DESY II they are produced by inserting a carbon fibre into the primary beam. The emerging bremsstrahlung is then converted into electrons and positrons using a metal plate converter. A magnet system then extracts the particles with desired properties.

Table 1 summarizes the data we took and the fraction that we managed to reconstruct within the given time frame of the summer student program. At CERN, we recorded approximately one million events per threshold and energy setting. The SPS serves as a pre-accelerator for the LHC so that the average event rate delivered in approximately ten second spills every minute was quite limited. Much higher average event rates were available at the continuous DESY beam so that more than five million events per setting were recorded there. Unfortunately, none of the DESY data could be analyzed due to the time

CERN SPS pion test beam						
E/GeV	Threshold setting S/N					
	5	6	7	8	9	10
120	✓	✓	✓	✓	✓	✓
80	✓	✓		✓		

DESY II electron test beam						
E/GeV	Threshold setting S/N					
	5	6	7	8	9	10
2	✓	✓	✓	✓	✓	✓
3	✓	✓	✓	✓	✓	✓
4	✓	✓	✓	✓	✓	✓

Table 1: A list of data sets that were taken at CERN and DESY during a data taking period of four weeks in total. Green check marks denote data sets that were recorded as well as reconstructed while red check marks denote data sets that were recorded but due to the time constraint not analyzed. The available test beam time of two weeks at CERN passed before all data for 80 GeV was collected.

constraint. The results presented in this report will be restricted to the CERN data that was taken with 120 GeV beam settings since the 80 GeV threshold scan was not completed. Moreover, the data quality of the reconstructed 80 GeV data could not be thoroughly verified during our stay at DESY.

5 Results

As mentioned above, the presentation of results will be restricted to CERN test beam data for a beam energy of 120 GeV.

5.1 Residual Distributions

Figure 8 shows the complete set of residual distributions for one threshold setting ($S/N = 8$) and the x direction. The corresponding plots for the y direction are depicted in figure 9 and for completeness, the distributions for all other threshold settings can be found in appendix A. A standard Gaussian χ^2 minimization fit using the default algorithm implemented in ROOT ([14]) was performed to obtain the widths of the distribution. The assumption that the distributions can be well described by Gaussian distributions can evidently be validated by the measurements. Furthermore, there is sufficient statistics to determine the widths of the distributions accurately. The relative errors on the obtained widths are well below the one percent level and the distributions are well centered around zero.

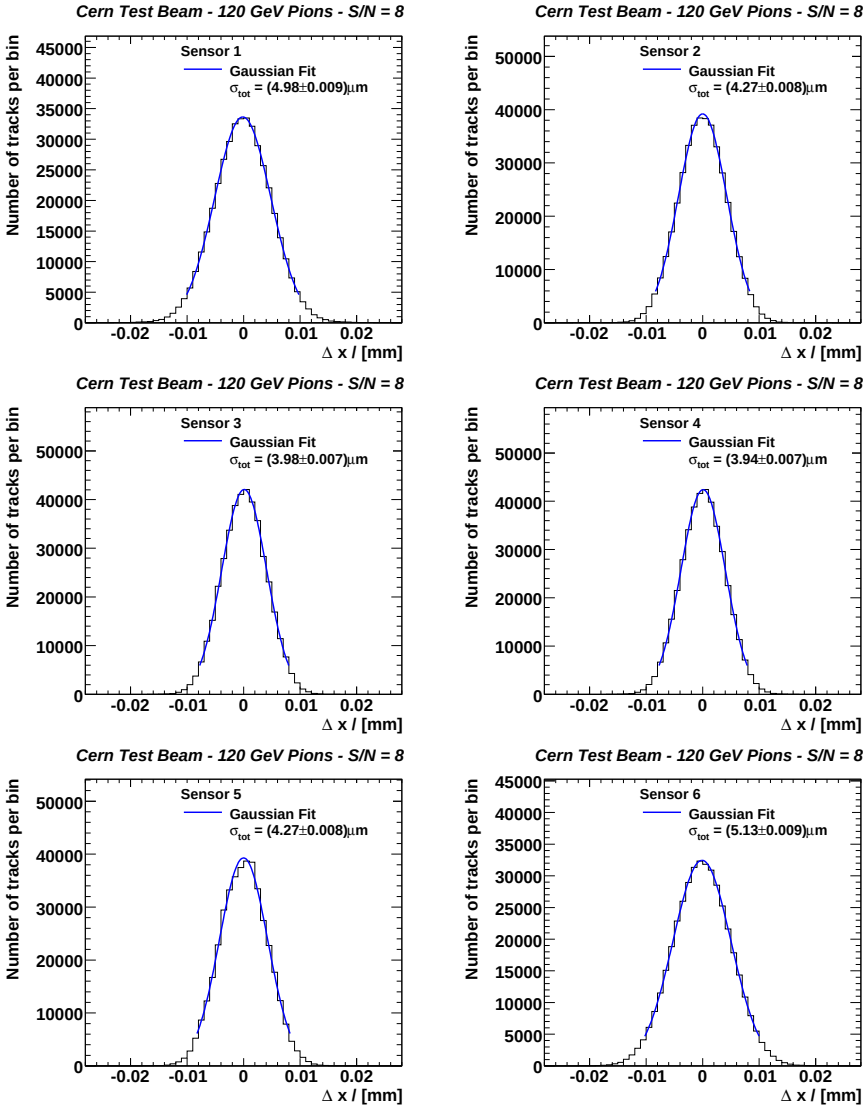

Figure 8: x residual distributions for threshold setting $S/N = 8$. Also given in the plots are the fit results including the widths of the distributions σ_{tot}.

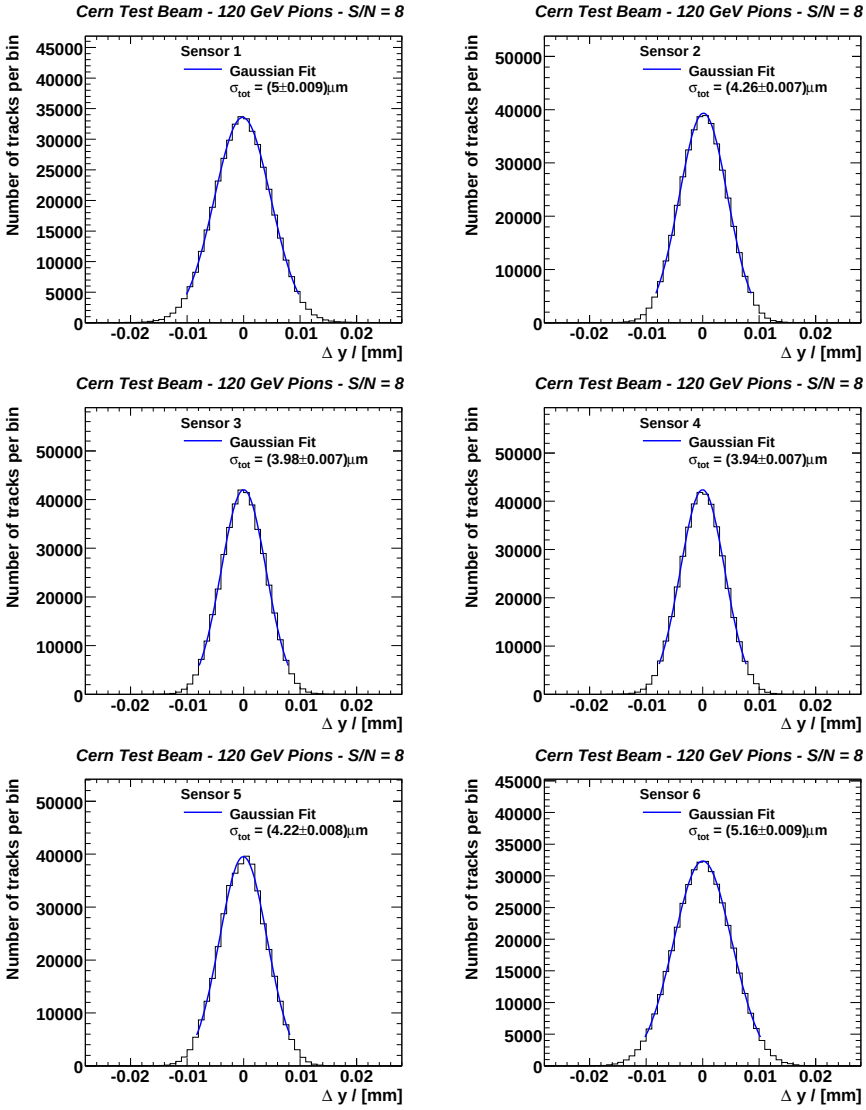

Figure 9: y residual distributions for threshold setting $S/N = 8$. Also given in the plots are the fit results including the widths of the distributions σ_{tot}.

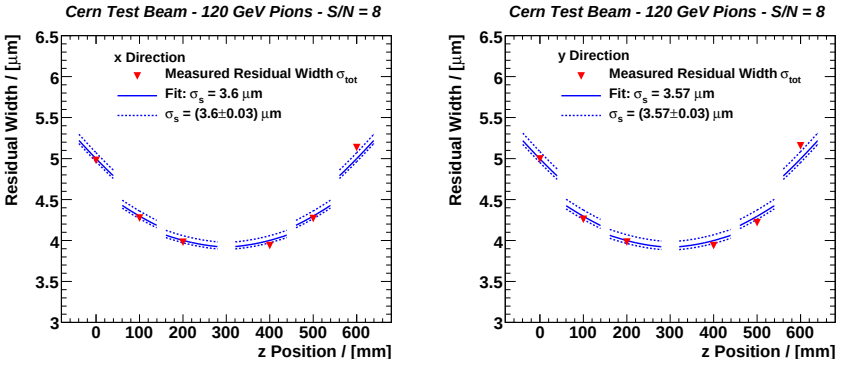

Figure 10: The total x and y residual widths for all six sensor planes plotted versus the respective z positions in the geometric setup of the telescope. Error bars are included but very small and hence not visible in the plots. The prediction of the total residual width according to equation (11) assuming the sensor resolution σ_s that is obtained from a fit is given in terms of the solid blue line. The corresponding error bands are denoted by dashed blue lines.

5.2 Extracting the Pointing and Sensor Resolution

As outlined in section 4.1, the total width of the residual distributions are related to the sensor resolution via

$$\sigma_\mathrm{tot}^2 = \sigma_\mathrm{tel}^2(\sigma_\mathrm{s}) + \sigma_\mathrm{s}^2 \tag{12}$$

where $\sigma_\mathrm{tel}(\sigma_\mathrm{s})$ is given in terms of the diagonal element of the matrix $\mathcal{M}^{-1}$ corresponding to the respective sensor plane. In that sense, we have an analytic expression for σ_tot with σ_s as a free parameter. From the six measured residual widths corresponding to one threshold setting one can thus obtain σ_s by a fit. The result of such a fit is visualized in figure 10. As can be seen in the depicted plots, the measured widths can be described very well by expression (12) and the relative errors on σ_s are just below the one percent level. Appendix B includes similar plots for the remaining threshold settings. The measurements from the y and x residuals agree very well, as can be seen in figure 11 in more detail. The overall result of the threshold scan for the 120 GeV test beam is given in figure 12 where not only the sensor resolution is given but also the telescope's pointing resolution as a function of the threshold setting. Over the entire threshold range a pointing resolution below 2 µm is achieved.

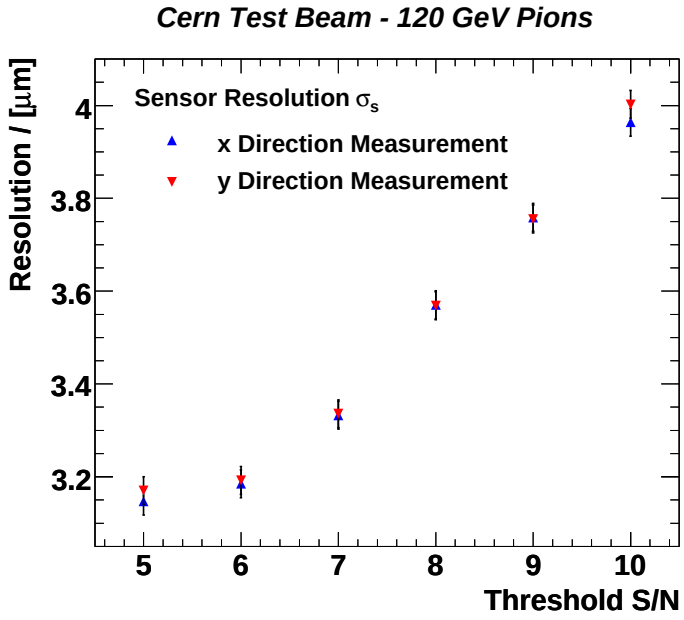

Figure 11: Comparison between x and y direction measurements. The obtained sensor resolutions agree very well within the uncertainties.

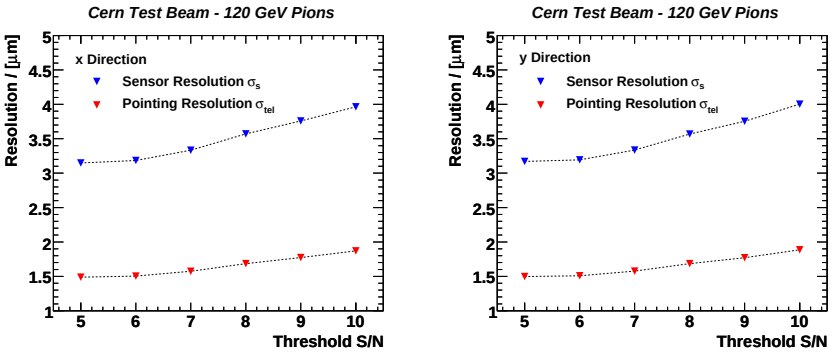

Figure 12: Measured sensor and telescope resolution dependence for the entire threshold range that was probed. Error bars are included but not visible due to their small size.

6 Summary and Outlook

In the presented analysis, the pointing resolution of the EUDET pixel telescope and its dependence on the threshold settings at a beam energy of 120 GeV was measured with an accuracy of less than 2 %. The measurement was based on the measurement of residual distributions, who's shape was confirmed to be Gaussian. Furthermore, a good agreement between the individual measurements of x- and y-direction measurements was observed. The presented approach of describing the observed residual widths and the telescope's pointing resolution in terms of the telescope geometry, the sensor thickness, and the sensor resolution turned out to be accurate in the sense that the data was well described and the fit errors on σ_s were small.

Due to the time constraint, the DESY test beam data could not be analyzed. This is particularly unfortunate since this would have given the opportunity to probe a different energy regime with beam energies one order of magnitude smaller. Increased multiple scattering effects must be expected to have an impact on the resolution power of the telescope at such small energies. If the track fitting approach used in the offline analysis properly accounts for those effects and if the data is still well described by the methods applied in this analysis could be answered by an analysis of the DESY data.

7 Acknowledgments

First and foremost I would like to thank my official supervisor Dr. Ingrid-Maria Gregor as well as Dr. Igor Rubinsky for their very time consuming supervision of our project at DESY. It is due to their commitment and patience that I was able to learn as much as I did during my time as a summer student.

We also received a lot of support from all other group members who were always willingly offering their help when we encountered problems or had open questions of any kind.

Finally, I would like to thank everyone who helped covering shifts in the control room during the four weeks of data taking. Without this massive support, we could have never taken as much data as we analyzed and presented in this report.

Bibliography

References

[1] T. Haas. "A pixel telescope for detector R&D for an international linear collider". In: *Nuclear Instruments and Methods in Physics Research A* 569 (1 2006). DOI: DOI:10.1016/j.nima.2006.09.011.

[2] A.F. Zarnecki and P. Niezurawski. *EUDET Telescope Geometry and Resolution Studies*. EUDET-Report-2007-01. arXiv:physics/0703058v1.

[3] J. Behr. *Test Beam Measurements with the EUDET Pixel Telescope*. EUDET-Report-2010-01. Retrieved on Sep. 8, 2011. URL: http://www.eudet.org/e26/e26/e27/e107291/eudet-report-2010-01.pdf.

[4] D. Cussans. *Description of the JRA1 Trigger Logic Unit*. EUDET-Memo-2008-50. Retrieved on Sep. 8, 2011. URL: http://www.eudet.org/e26/e28/e615/e839/eudet-memo-2008-50.pdf.

[5] A.C. Ramusino. *The EUDET Data Reduction Board*. EUDET-Memo-2008-38. Retrieved on Sep. 8, 2011. URL: http://www.eudet.org/e26/e28/e615/e814/eudet-memo-2008-38.pdf.

[6] EUDAQ software hompage. Retrieved on Sep. 8, 2011. URL: http://projects.hepforge.org/eudaq/.

[7] I. Rubinsky. *EUTelescope offline track reconstruction and DUT analysis software*. EUDET-Memo-2010-12. Retrieved on Sep. 8, 2011. URL: http://www.eudet.org/e26/e28/e86887/e107460/EUDET-Memo-2010-12.pdf.

[8] I. Bulgheroni et al. *EUTelescope: tracking software*. EUDET-Memo-2007-20. Retrieved on Sep. 8, 2011. URL: http://www.eudet.org/e26/e28/e182/e425/eudet-memo-2007-20.pdf.

[9] F. Gaede and J. Engels. *Marlin et al - A Software Framework for ILC detector R&D*. EUDET-Report-2007-11. Retrieved on Sep. 8, 2011. URL: http://www.eudet.org/e26/e27/e584/eudet-report-2007-11.pdf.

[10] Millepede II software hompage. Retrieved on Sep. 8, 2011. URL: https://www.wiki.terascale.de/index.php/Millepede_II.

[11] K. Nakamura et al. "Review of Particle Physics". In: *Journal of Physics G: Nuclear and Particle Physics* 37.7A (2010).

[12] DESY test beam homepage. Retrieved on Sep. 8, 2011. URL: http://adweb.desy.de/~testbeam/.

[13] Informations on the CERN secondary beam lines, Experimental Areas (EA) Group. Retrieved on Sep. 8, 2011. URL: http://sl.web.cern.ch/SL/eagroup/beams.html.

[14] ROOT hompage. Retrieved on Sep. 8, 2011. URL: http://root.cern.ch.

A Residual Distributions

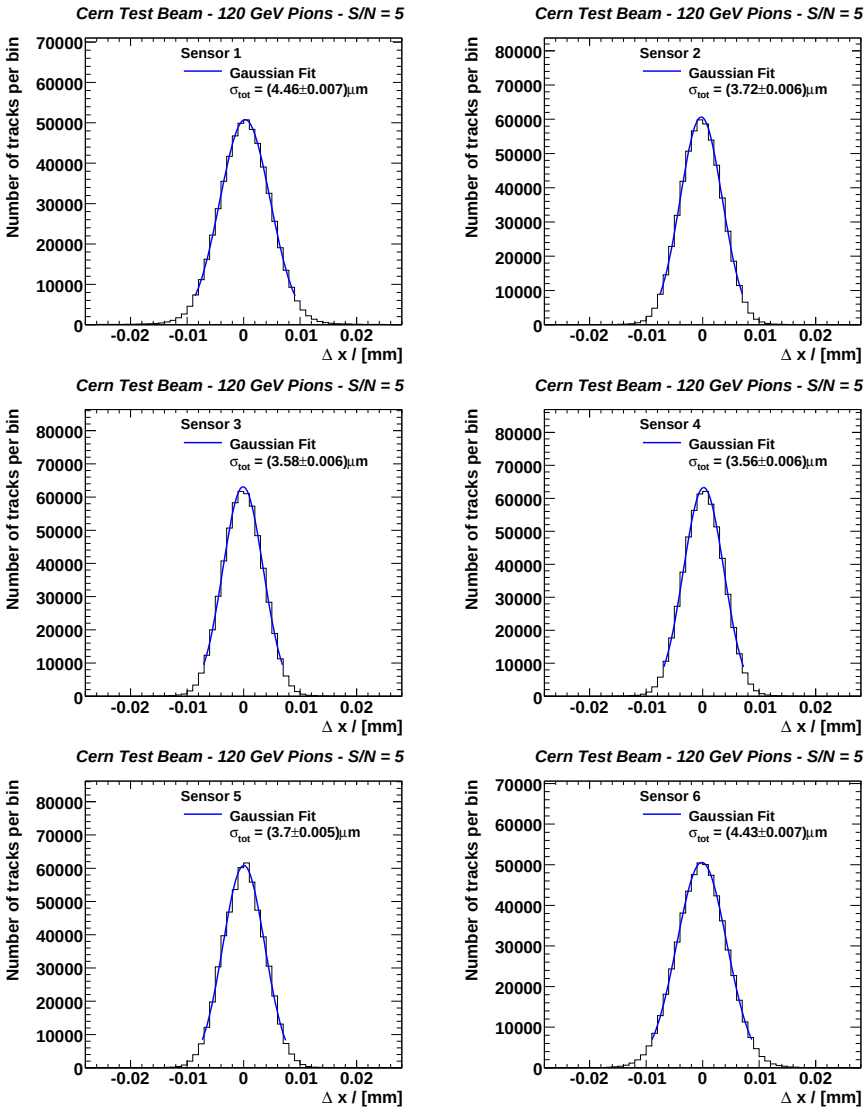

Figure 13: x residual distributions for threshold setting $S/N = 5$.

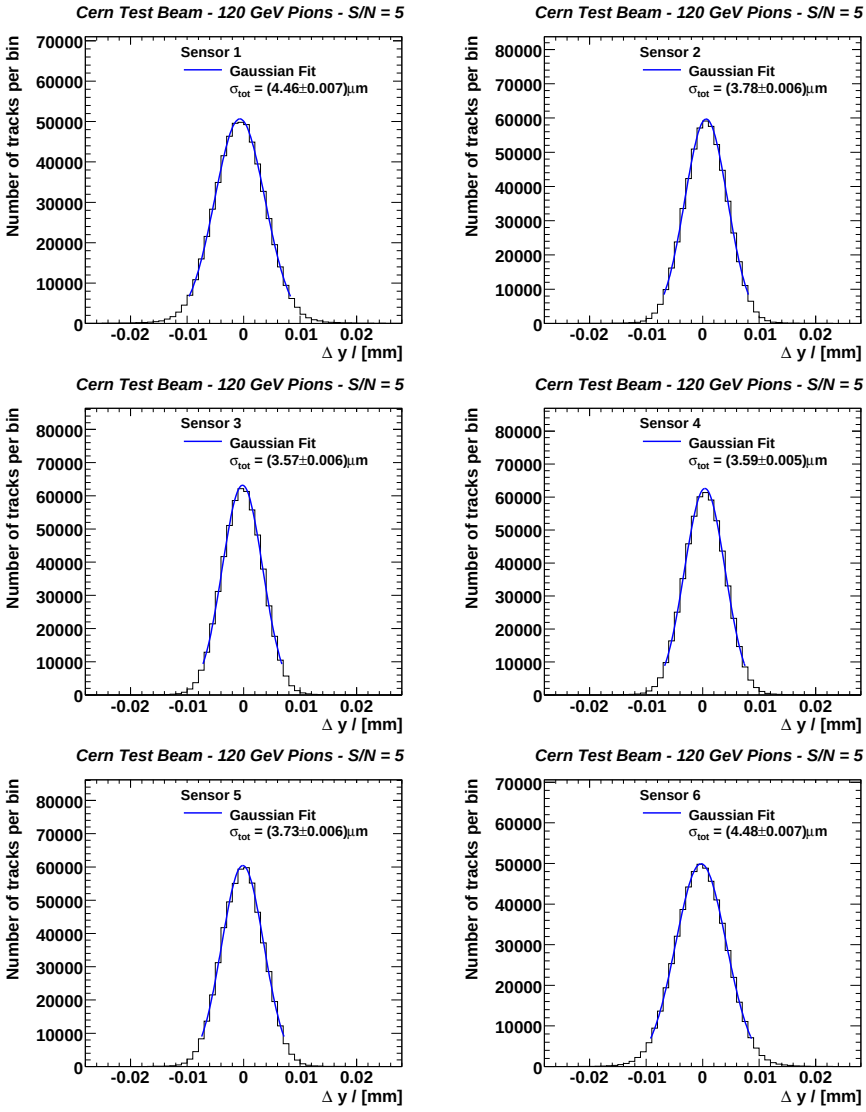

Figure 14: y residual distributions for threshold setting $S/N = 5$.

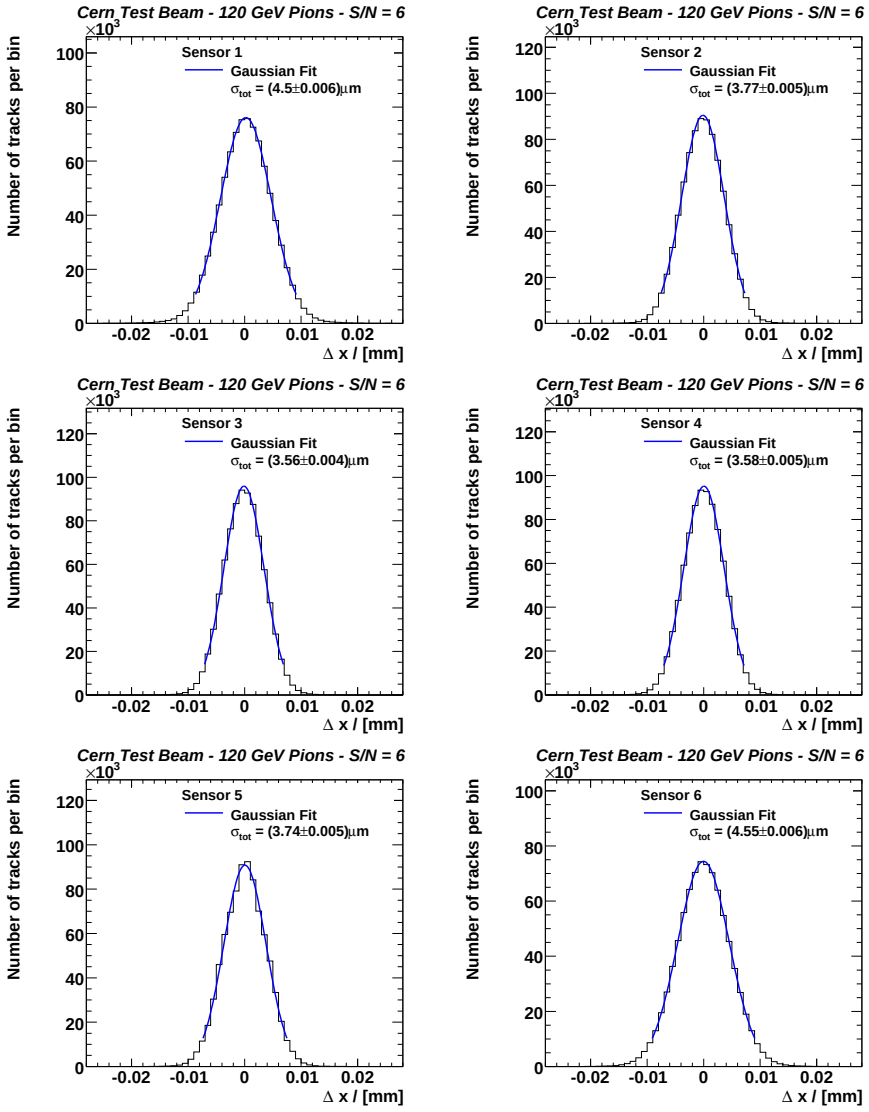

Figure 15: x residual distributions for threshold setting $S/N = 6$.

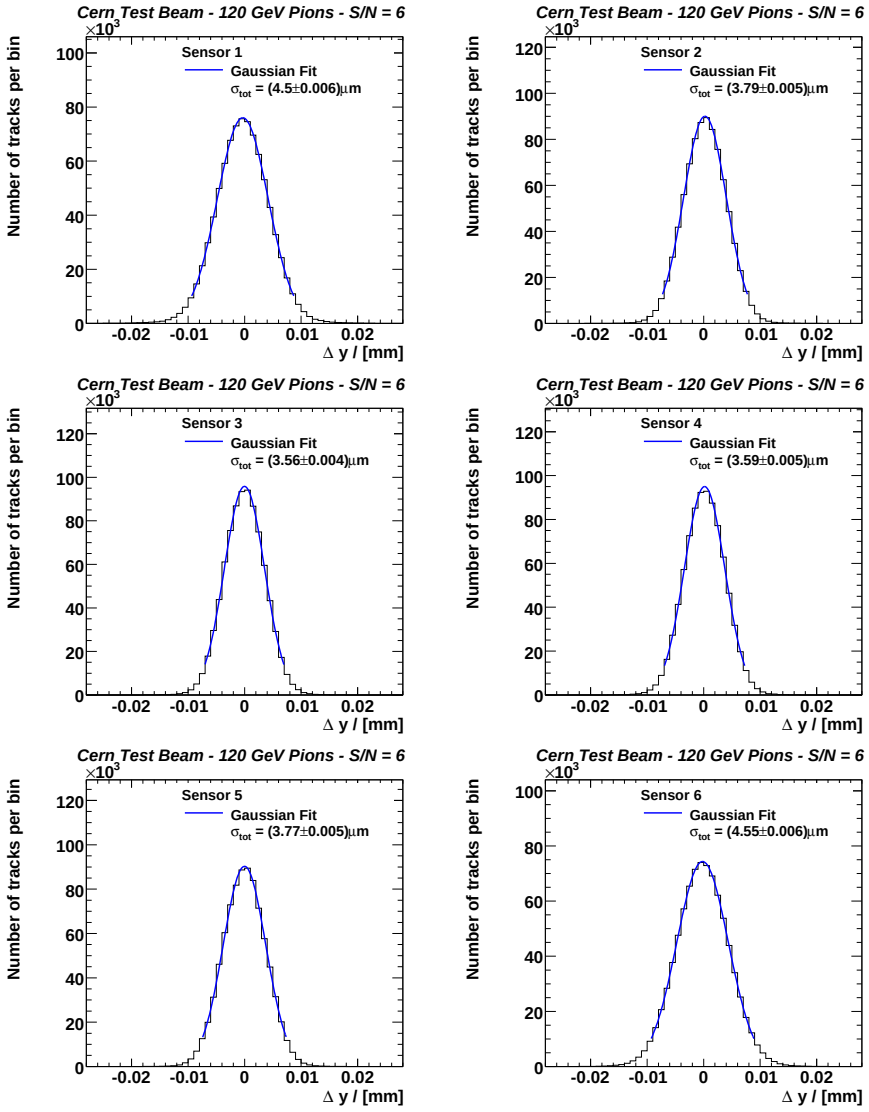

Figure 16: y residual distributions for threshold setting $S/N = 6$.

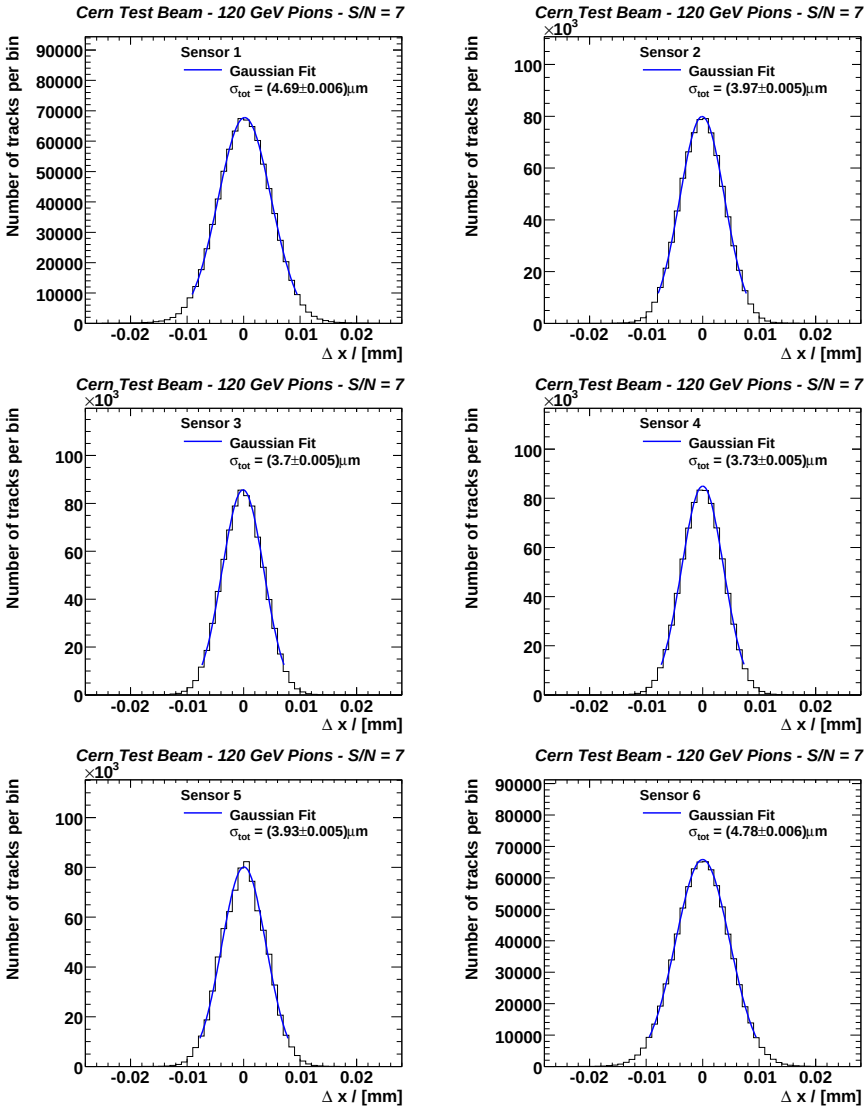

Figure 17: x residual distributions for threshold setting $S/N = 7$.

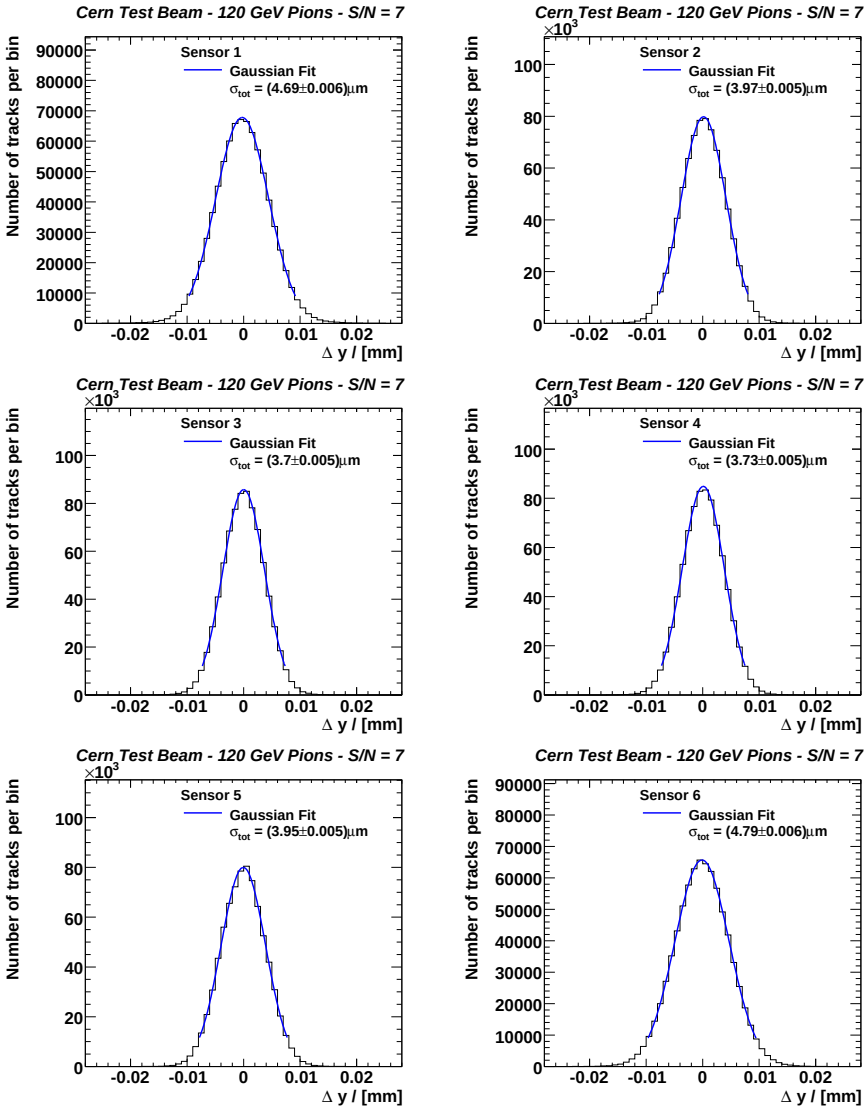

Figure 18: y residual distributions for threshold setting $S/N = 7$.

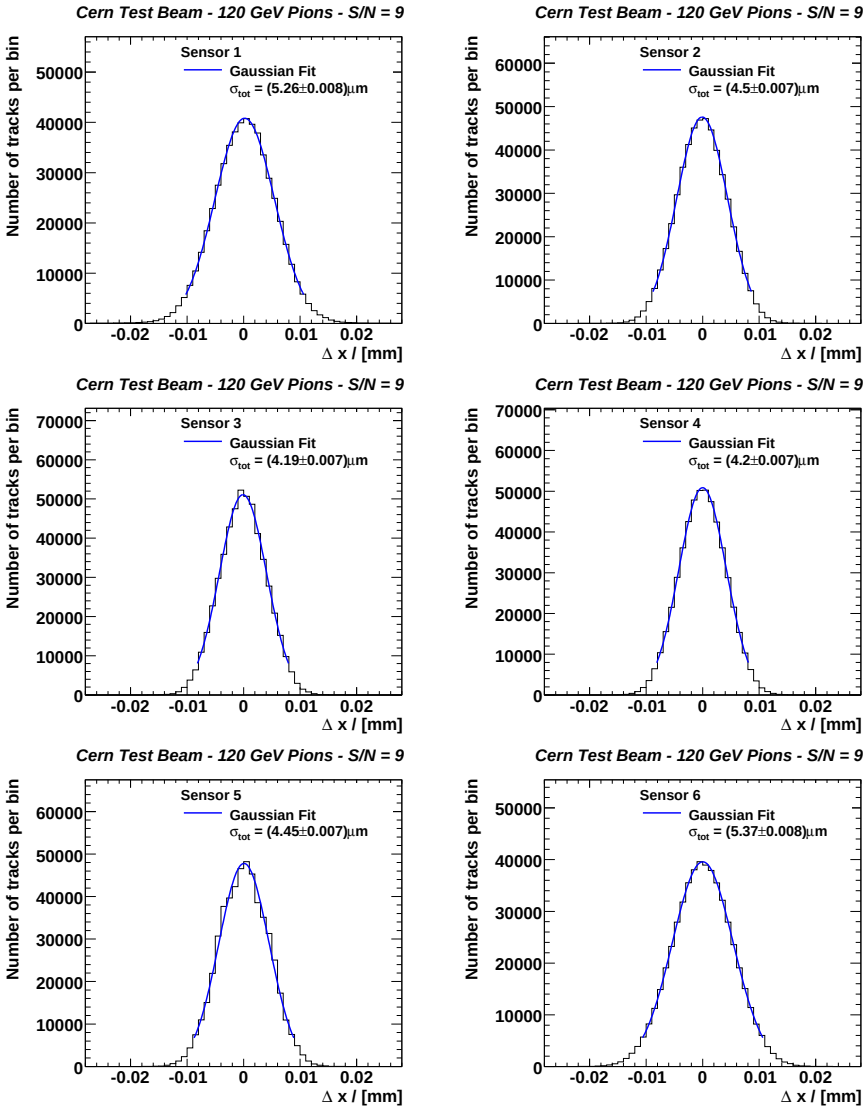

Figure 19: x residual distributions for threshold setting $S/N = 9$.

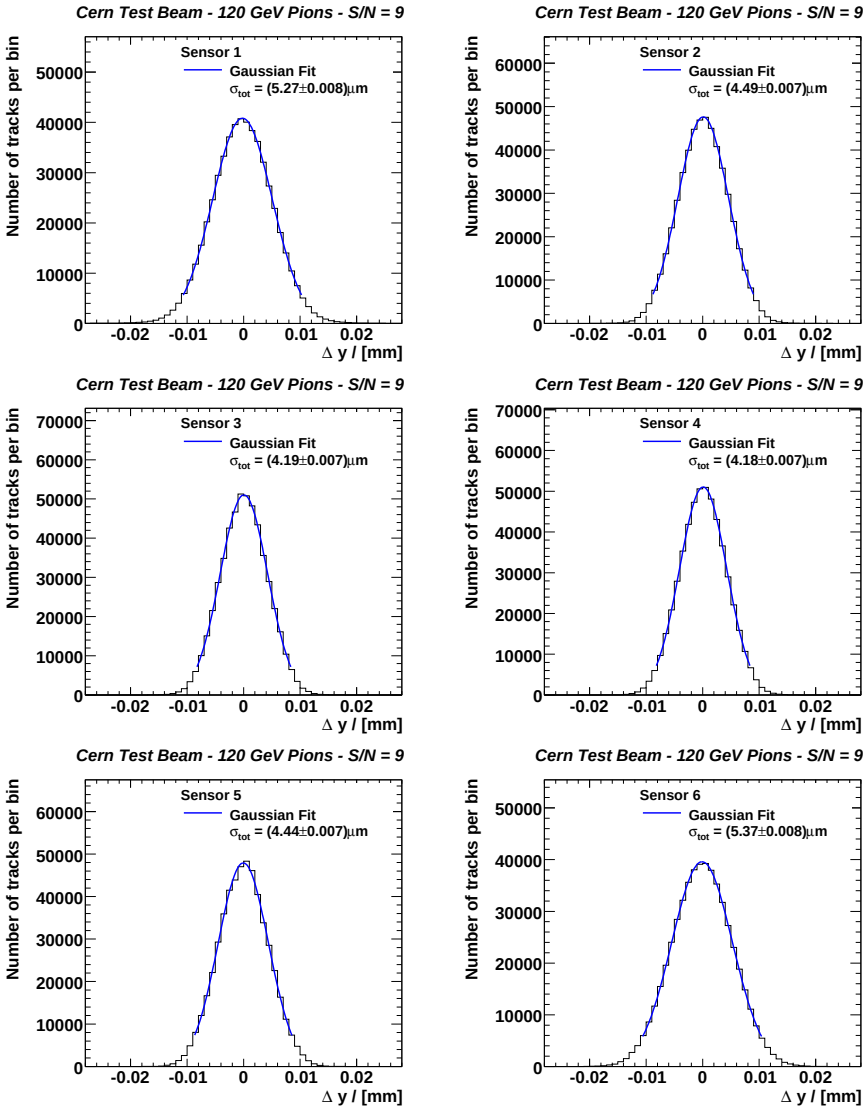

Figure 20: y residual distributions for threshold setting $S/N = 9$.

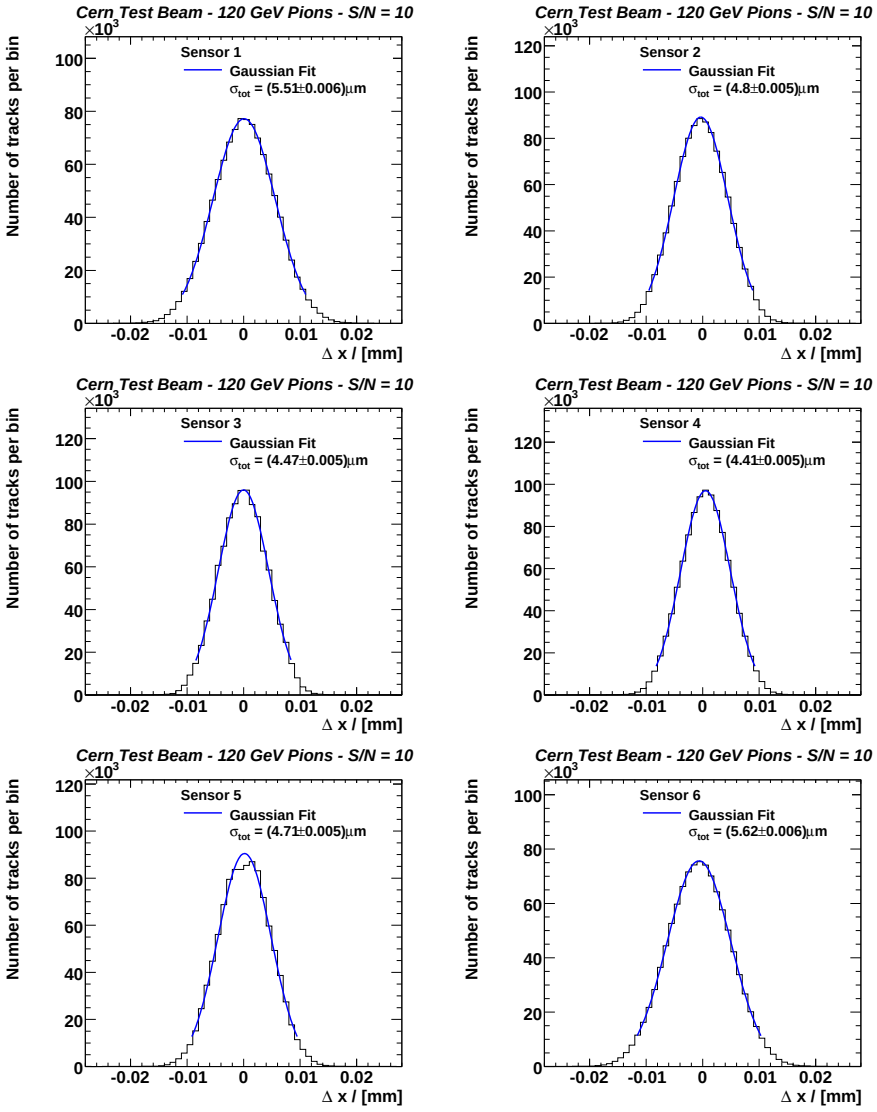

Figure 21: x residual distributions for threshold setting $S/N = 10$.

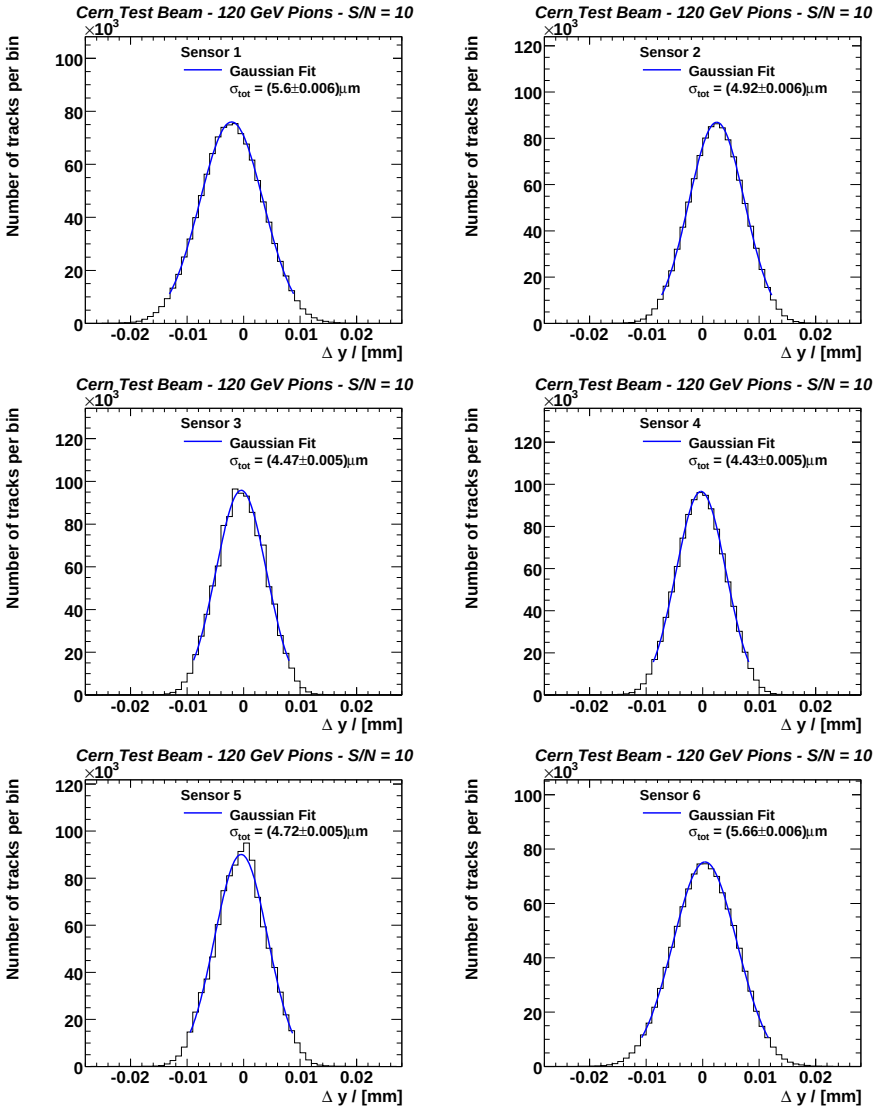

Figure 22: y residual distributions for threshold setting $S/N = 10$.

B Plots for the Extraction of σ_s

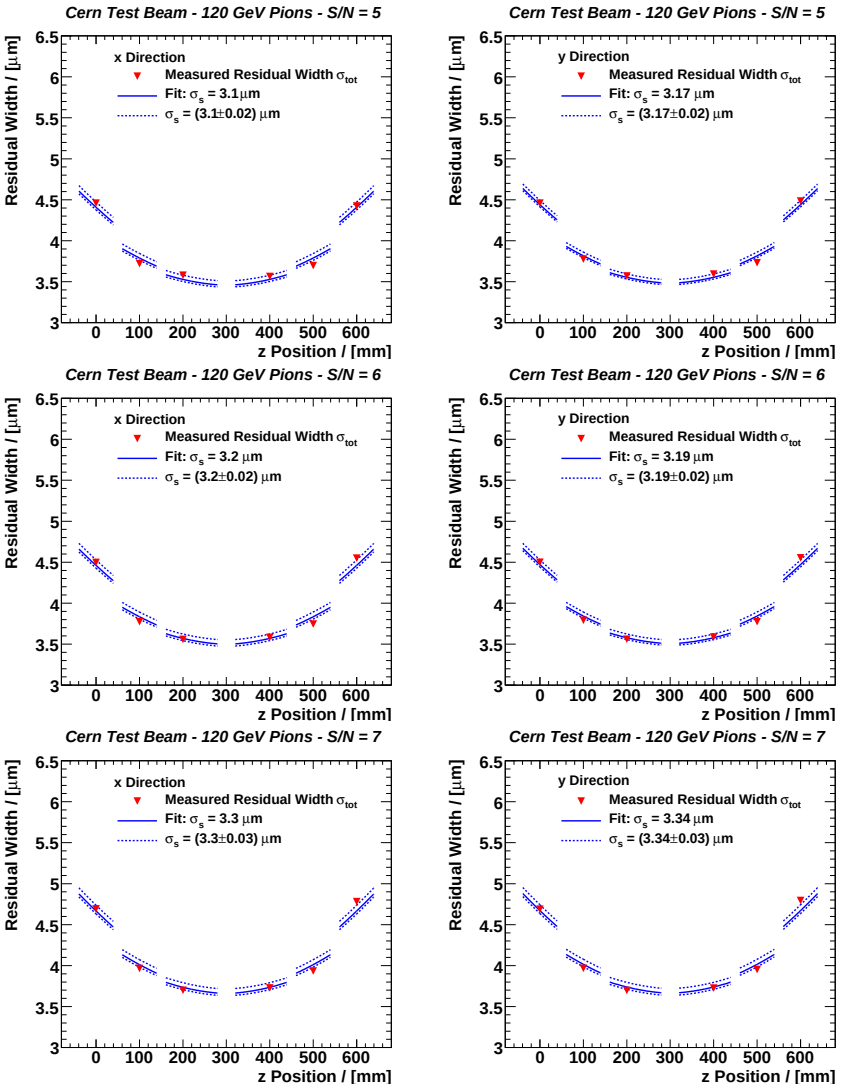

Figure 23: The total x and y residual widths for threshold settings $S/N = 5$ to $S/N = 7$.

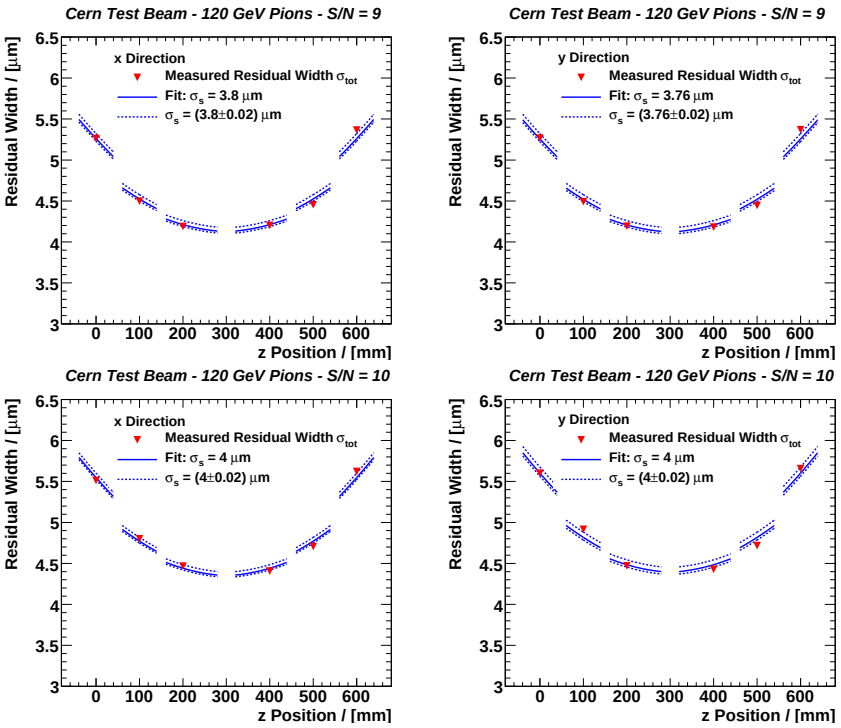

Figure 24: The total x and y residual widths for threshold settings $S/N = 9$ an $S/N = 10$.